Chemical Geology 269 (2010) 52–61

Contents lists available at ScienceDirect

Chemical Geology

journal homepage: www.elsevier.com/locate/chemgeo

Phosphorus and iron cycling in deep saprolite, Luquillo Mountains, Puerto Rico

Heather L. Buss [a,*], Ryan Mathur [b], Arthur F. White [a], Susan L. Brantley [c]

[a] U.S. Geological Survey, 345 Middlefield Rd., MS 420, Menlo Park, CA 94040, United States
[b] Department of Geology, Juniata College, Huntingdon, PA 16652, United States
[c] Earth and Environmental Systems Institute, The Pennsylvania State University, University Park, PA 16802, United States

ARTICLE INFO

Article history:
Accepted 3 August 2009

Keywords:
Phosphorus
Iron isotopes
Saprolite
Apatite weathering rate
Fe(II)-oxidizing bacteria

ABSTRACT

Rapid weathering and erosion rates in mountainous tropical watersheds lead to highly variable soil and saprolite thicknesses which in turn impact nutrient fluxes and biological populations. In the Luquillo Mountains of Puerto Rico, a 5-m thick saprolite contains high microorganism densities at the surface and at depth overlying bedrock. We test the hypotheses that the organisms at depth are limited by the availability of two nutrients, P and Fe. Many tropical soils are P-limited, rather than N-limited, and dissolution of apatite is the dominant source of P. We document patterns of apatite weathering and of bioavailable Fe derived from the weathering of primary minerals hornblende and biotite in cores augered to 7.5 m on a ridgetop as compared to spheroidally weathering bedrock sampled in a nearby roadcut.

Iron isotopic compositions of 0.5 N HCl extracts of soil and saprolite range from about $\delta^{56}Fe = 0$ to $-0.1‰$ throughout the saprolite except at the surface and at 5 m depth where $\delta^{56}Fe = -0.26$ to $-0.64‰$. The enrichment of light isotopes in HCl-extractable Fe in the soil and at the saprolite–bedrock interface is consistent with active Fe cycling and consistent with the locations of high cell densities and Fe(II)-oxidizing bacteria, identified previously. To evaluate the potential P-limitation of Fe-cycling bacteria in the profile, solid-state concentrations of P were measured as a function of depth in the soil, saprolite, and weathering bedrock. Weathering apatite crystals were examined in thin sections and an apatite dissolution rate of 6.8×10^{-14} mol m^{-2} s^{-1} was calculated. While surface communities depend on recycled nutrients and atmospheric inputs, deep communities survive primarily on nutrients released by the weathering bedrock and thus are tightly coupled to processes related to saprolite formation including mineral weathering. While low available P may limit microbial activity within the middle saprolite, fluxes of P from apatite weathering should be sufficient to support robust growth of microorganisms in the deep saprolite.

Published by Elsevier B.V.

1. Introduction

Except where recent landslides have occurred, thick saprolites in the Luquillo Mountains isolate the weathering bedrock from the soil ecosystem. Despite high precipitation (>4000 mm $year^{-1}$) in the Rio Icacos watershed of the Luquillo Mountains, most water that reaches the soil moves through the shallow soil layers and the water that does infiltrate to the deep saprolite on the ridges does so slowly: 1.8–2.6 m $year^{-1}$ (Turner, 2001). Established tropical forests are typically characterized by a closed nutrient cycle in which nutrients are tightly cycled within the surface soil and biomass because the underlying substrates are highly weathered and thus nutrient poor (e.g., Bruijnzeel, 1991). The majority of nutrients in precipitation and dry deposition in the Rio Icacos watershed are thus likely rapidly scavenged by the abundant tropical vegetation and soil organisms, leaving little to infiltrate to subsurface communities, as evidenced by very low DOC concentrations in the deep saprolite porewaters (Murphy, 1995). Indeed, tracers such as Sr and Si isotope ratios and Si/Ge ratios indicate that while vegetation and porewaters in the soil and shallow saprolite of the Rio Icacos watershed contain atmospherically derived elements, middle and deep saprolite porewaters (collected from nested suction water samplers) are dominated by elements derived from bedrock weathering (Kurtz and Derry, 2004; Ziegler et al., 2005; Pett-Ridge et al., 2009; Lugolobi et al., 2006). Furthermore, the majority of the annual precipitation falls as short, intense storm events during which runoff to the streams occurs through the shallow saprolite only (Lugolobi et al., 2006). Deeper saprolite microbial communities are therefore highly dependent upon weathering bedrock for nutrients (Buss et al., 2005). In the deep saprolite of the Rio Icacos watershed, cell densities increase near the bedrock–saprolite interface where Fe(II)-oxidizing bacteria were detected. Maximum growth rates were estimated for these chemolithoautotrophic microorganisms and for their dependent heterotrophic communities based on the rate of release of Fe(II) from silicate minerals during weathering at the bedrock–saprolite interface (Buss et al., 2005). In Buss et al. (2005), cell densities (live + dead) in the

* Corresponding author. Tel.: +1 650 329 4420; fax: +1 650 329 4538.
E-mail address: hlbuss@usgs.gov (H.L. Buss).

0009-2541/$ – see front matter. Published by Elsevier B.V.
doi:10.1016/j.chemgeo.2009.08.001

saprolite were estimated by direct counting and from DNA yields. The activity of the microorganisms was not examined and it is possible that the organisms present at depth were merely dormant due to P-limitation. In this paper, we compare P fluxes and P requirements to growth rates based on Fe(II) fluxes to test whether the community at depth in these samples was nutrient (P)-limited or energy (Fe(II))-limited. We also use Fe isotopes to examine the activity of Fe-cycling microorganisms in the saprolite profile.

Phosphorus is an essential macronutrient, vital to all biological systems. Adenosine triphosphate (ATP), one of the most important and abundant biomolecules in nature, is formed during photosynthesis and cellular respiration and functions as an energy shuttle, providing chemical energy for biosynthesis, cell motility, and osmotic transport of molecules through cell membranes (Garrett and Grisham, 1999). Phosphorus is found in DNA and RNA as phosphate ester bridges that link individual nucleotides, in cell membranes as phospholipids, and as a component of many signaling molecules, enzymes, and coenzymes (Frausto da Silva and Williams, 1991; Garrett and Grisham, 1999). However, P availability is commonly very low in tropical soils, a fact that is often attributed to the strong sorption of P to Fe and Al oxides (e.g., Sanchez, 1976; Vitousek, 1984; Olander and Vitousek, 2005). In contrast, tropical soils are typically not N-limited (e.g., Vitousek and Sanford, 1986). In the tropical Luquillo Mountains of northeastern Puerto Rico, low rates of NO_3^- leaching and export (McDowell and Asbury, 1994) result primarily from effective N retention via dissimilatory nitrate reduction to ammonium (Templer et al., 2008). High rates of NH_4^+ production via rapid decomposition of soil organic matter also contribute to N availability and retention in tropical soils (Vitousek and Sanford, 1986). In saprolite porewaters in the Rio Icacos watershed, N concentrations increase with depth on both ridgetops and slopes (White et al., 1998) suggesting that, like soils, deep saprolite is also not N-limited. It is interesting to note that of the two elements that are most often limiting in terrestrial systems, N and P, only P comes directly from rocks (Wardle et al., 2004).

Pools of P in a forest soil may include primary minerals (predominantly apatite), secondary minerals (associated with Fe or Al oxides or clays), aqueous species in porewaters (inorganic or organic complexes), and solid organic P (contained in biomass and other organic matter). External sources of P to a soil system include bedrock weathering and atmospheric deposition (precipitation and dust). Most of the P associated with secondary minerals, biomass, and organic matter represent internal sources of P that are recycled and transferred between pools on various timescales during the lifetime of an ecosystem. In most soil profiles, P is supplied into the system almost entirely by weathering due to low atmospheric input of P (Walker and Syers, 1976). However, Caribbean island soils receive significant nutrient inputs from African dust and volcanic ash (Graham and Duce, 1982; Heartsill-Scalley et al., 2007; Muhs et al., 2007). Thick, highly weathered saprolites on the ridges of the Luquillo Mountains of Puerto Rico effectively isolate surface soils from weathering bedrock (e.g., Buss et al., 2005), thus atmospheric deposition may dominate exogenous input of P to the ridgetop soils (Pett-Ridge, 2009). In contrast, mineral weathering is expected to dominate P input to deep saprolite or where saprolite is thin due to topography or erosion. Landslides, which are the dominant mechanism of erosion in the Luquillo Mountains (Simon et al., 1990), increase access to mineral-derived nutrients, notably apatite, which affects the rate of vegetation re-growth on landslide scars (e.g., Zarin and Johnson, 1995; Frizano et al., 2002).

Stable Fe isotopes provide a promising new tool for tracing biogeochemical Fe cycles in soils and weathering systems. Iron isotope systematics have been studied for multiple processes that are relevant to soil systems including i) inorganic dissolution (mobilization of Fe from minerals by H^+), ii) organic dissolution (mobilization of Fe by organic ligands or microorganisms), iii) reductive dissolution (reduction of mineral-bound Fe(III) followed by mobilization of Fe(II)), iv) precipitation of Fe(III)-(hydr)oxides from solution, v) adsorption of Fe onto oxide or clay minerals, and vi) uptake of Fe by plants or microorganisms. Fractionations favoring the release of the light isotope (^{54}Fe) to solution leaving an isotopically heavy solid (enriched in ^{56}Fe) have been documented for organic dissolution of hornblende by bacteria, organic acids, and siderophores (Brantley et al., 2001b, 2004) and for ligand-controlled Fe relocation in soils (Wiederhold et al., 2007b). Organic dissolution of goethite did not produce an isotopic fractionation (Brantley et al., 2004), nor did inorganic dissolution of hornblende or goethite (Brantley et al., 2001b, 2004). Reductive dissolution of goethite, hematite, and ferrihydrite in the presence of bacteria generates a solution that is isotopically light with respect to the starting mineral (e.g., Beard et al., 1999, 2003; Icopini et al., 2004; Crosby et al., 2005, 2007), which leads to a loss of isotopically light Fe from soils (Thompson et al., 2007; Wiederhold et al., 2007b). However, fractionation may occur via isotopic exchange between aqueous Fe (II) and sorbed Fe(II), rather than during reductive dissolution, because adsorption of Fe(II) onto goethite preferentially removes ^{56}Fe from solution, with or without bacteria (Brantley et al., 2004; Icopini et al., 2004). Similarly, precipitation of ferrihydrite also concentrates the heavier isotope in a solid product while the solution becomes isotopically lighter (Bullen et al., 2001; Teutsch et al., 2005). Plants that obtain Fe by acidifying the rhizosphere to promote reductive dissolution of Fe(III)-oxides preferentially take up Fe that is isotopically light relative to the surrounding soil (Guelke and Von Blanckenburg, 2007). In contrast, uptake of Fe(III)–sideorphore complexes does not result in a fractionation of Fe in grasses that produce phytosiderophores (Guelke and Von Blanckenburg, 2007).

Here we use Fe isotope ratios to investigate controls on the bioavailable fraction of Fe. Iron isotopes are measured in the fraction of Fe liberated from soil and saprolite samples by a dilute HCl leach, which is often associated with the most reactive, or bioavailable, fraction of Fe in soils and sediments (e.g., Fantle and DePaolo, 2004; Buss et al., 2005; Severmann et al., 2006; Wiederhold et al., 2007b). In addition to colloid-bound Fe, organic-bound Fe, and the (typically minute) aqueous Fe(II), it is this "reactive Fe" that is transported from weathering profiles to rivers and oceans and dominates the Fe isotope signatures of these bodies of water (Fantle and DePaolo, 2004). In high silicate soils, Fe within this reactive pool is expected to be isotopically light relative to bedrock and residual material (Fantle and DePaolo, 2004; Wiederhold et al., 2007b), which may indicate active biogeochemical cycling of Fe. For example, complexation of Fe by organic ligands or reductive dissolution of Fe(III)-(hydr)oxides would cause an excursion towards a lighter Fe isotope signature within the reactive Fe pool, while Fe uptake by vegetation would likely yield a heavier Fe isotope signature (Fantle and DePaolo, 2004; Wiederhold et al., 2006, 2007a,b). In soils or regolith where the residual (non-HCl-extractable) Fe is dominated by Fe(III)-hydroxides, isotopic distinction between the two pools may be less than in silicate soils due to rapid isotopic exchange between sorbed Fe(II) and Fe(III)-hydroxides (Pedersen et al., 2005). Here we test the hypothesis that HCl-extractable Fe will be isotopically light in the biologically active zones of the Rio Icacos weathering profile, relative to zones in which biological activity is suppressed due to limited nutrient and energy fluxes.

2. Methods

2.1. Field site and sample collection

The Rio Icacos watershed in the Luquillo Experimental Forest of northeastern Puerto Rico is predominantly located in a lower montane wet colorado forest that receives over 4000 mm of rain annually. The watershed is underlain by the Rio Blanco quartz diorite

bedrock, which weathers spheroidally resulting in rounded corestones of about 2 m in diameter, surrounded by 0.2–2-m thick zones of concentric, partially weathered rock layers called rindlets (Turner et al., 2003; Buss et al., 2004; Buss et al., 2005; Fletcher et al., 2006; Buss et al., 2008). The rindlet zones are mantled by 200 ka regolith, dated using ^{10}Be (Brown et al., 1995), and is comprised of 2–8 m of saprolite and 0.5–1 m of highly weathered Picacho-Ciales complex soils, previously classified as Ultisols (Boccheciamp et al., 1977), but now considered Inceptisols due to weak B horizon development (USDA NCRS, 2002).

Two 5.7 cm diameter cores of soil and saprolite were collected 1 m apart by hand augering to 7.5 m and 5.0 m depth at the top of the Guaba Ridge in the Rio Icacos watershed (latitude 18°16.903′N, longitude 65°47.418′W), which has been mapped by others (Murphy et al., 1998; White et al., 1998; Turner et al., 2003; Buss et al., 2008). Samples were taken from the auger at 0.15–0.3 m depth intervals. The deeper core penetrated the rindlet zone below 5 m depth. The sampling procedure was described by Buss et al. (2005a). Redoximorphic features such as gleying or mottling were not observed in the saprolite samples, but several zones of pink and black Mn-oxide concentrations were identified (Buss et al., 2005). The saprolite is formed on a cuchillo, or knife-edge ridge, and is not significantly influenced by lateral flow of groundwater at depth (White et al., 1998; Lugolobi et al., 2006). The pH of the soil and saprolite porewater is 4.0–5.4 (White et al., 1998). The edge of a corestone and the complete 49 cm section of rindlets above the corestone were sampled at a nearby roadcut exposed on Route 191 (latitude 18°16.216′N, longitude 65°47.055′W), preserving the position and orientation of the individual rindlets as described by Buss et al. (2008). The corestone was located beneath about 2 m of saprolite forming a small local topographic high.

2.2. Phosphorus and apatite analyses

Phosphorus was measured by inductively coupled plasma atomic emission spectrometry (ICP-AES) after lithium metaborate fusion digestion (SGS Mineral Laboratories, Ontario, Canada) of pulverized and sieved (150 μm) corestone, rindlet, and saprolite samples. Apatite crystals were identified in thin sections of the corestone and rindlets using backscattered electron (BSE) imaging and energy dispersive X-ray spectrometry (EDS) on an FEI Quanta 400 SEM. Point counting of apatite crystals was performed on backscattered images using XT-Docu software (v. 3.2, Soft-Imaging System GmbH, Münster, Germany), which calculates the volume of each user-defined phase based on the backscatter grayscale value. This technique has been used to measure porosity and to point count mineral phases in weathering rocks (Dorn, 1995; Dixon et al., 2006; Buss et al., 2008).

2.3. Fe isotope analysis

Iron in soils and sediments exist in many different forms (e.g., as readily exchangeable ions; precipitated as, or bound to, oxide or hydroxide phases; bound to organic matter; in carbonates; or in silicates). These fractions are often extracted sequentially by stronger and stronger leaching procedures. Extractions are favored over total digests because only average isotope ratios of all different Fe phases are obtained from total digests. Extraction of soils and sediments with dilute HCl is expected to liberate readily exchangeable ions, adsorbed Fe, some organic-bound Fe, and poorly crystalline Fe oxides and hydroxides (Wiederhold et al., 2007b) and represent a more reactive, or bioavailable, Fe pool than the bulk solid (Emerson, 2002). Iron isotopes were measured in 0.5 N HCl extracts performed on soil and saprolite samples augered from the Guaba Ridge. Iron isotopes are not fractionated by this extraction procedure: fractionation did not occur during dissolution of goethite or hematite in 0.5 N HCl, even when dissolution was incomplete (Skulan et al., 2002; Wiederhold et al., 2006). Soil and saprolite samples were air dried and gently ground only to break up aggregates before sieving to 2 mm. Samples (0.5 g) were then combined with 10 ml 0.5 N HCl in 15 mL centrifuge tubes and agitated on an end-over-end shaker at room temperature for 17 h, followed by centrifugation at 4000 ×g for 10 min (Buss et al., 2005). Supernatants were decanted, centrifuged again, and filtered to 0.4 μm (SFCA-membrane syringe filter, Cole-Parmer). Concentrations of ferrous iron in the extracts were measured by ultraviolet–visible (UV/Vis) spectrophotometry as described and reported by Buss et al. (2005). Total Fe was measured by inductively coupled plasma mass spectrometry (ICP-MS) and ferric iron was calculated as the difference between total and ferrous iron concentrations, as detailed in Buss et al. (2005).

Iron was separated from other cations in the HCl extracts following a standard ion exchange column method using AG MP-1 (100–200 mesh) resin (BIORAD) as described by Brantley et al. (2004). Post-purification iron yield was measured volumetrically and found to be better than 95%. Fe isotopes were measured at Washington State University using a multi-collector inductively coupled plasma mass spectrometer (MC-ICP-MS, Neptune®, Thermo-Finnigan). The Fe concentration in each sample was adjusted to 3 ppm and a 3 ppm Cu standard was added to each. Sample measurements were bracketed with the standard–sample–standard technique. The mass bias in each sample was corrected using the exponential law (Arnold et al., 2004) and by using the graphical techniques developed by Maréchal et al. (1999). Both methods of data reduction resulted in values that were within the reported 2σ error (±0.1‰). This error was calculated by using multiple measurements of the Fe isotope ratio of goethite throughout four weeks of analysis (sample measured 25 times). The δ^{56}Fe (‰) values were calculated relative to the international Fe standard IRMM-014, using the following equation:

$$\delta^{56/54}\mathrm{Fe} = \left(\frac{\left(^{56}\mathrm{Fe}/^{54}\mathrm{Fe}\right)_{\mathrm{sample}}}{\left(^{56}\mathrm{Fe}/^{54}\mathrm{Fe}\right)_{\mathrm{IRMM}}} - 1 \right) \times 1000 \quad (1)$$

3. Results

To evaluate mass transfer (loss or gain of an element relative to the parent rock composition) of P in the Rio Icacos weathering profile, we calculate Ti-normalized solid-state concentrations of P, C_w, which may differ from the measured value, C, due to changes in density and concentrations of other elements during weathering:

$$C_w = C\left(\frac{C_{Ti,p}}{C_{Ti,w}}\right) \quad (2)$$

where $C_{Ti,p}$ (mol kg^{-1}) is the solid-state concentration of Ti in the protolith and $C_{Ti,w}$ is the solid-state concentration of Ti in the weathered material (Ti measured by ICP-AES). Open-system mass transport (e.g., Brimhall and Dietrich, 1987; Anderson et al., 2002) is quantifiable in the Rio Icacos weathering profiles because the protolith is homogenous, of uniform age, and contains a relatively inert component that persists in the weathered material (Chadwick et al., 1990). White et al. (1998) and Buss et al. (2008) identified Ti as relatively immobile in the Rio Icacos saprolite relative to the bedrock based on calculations of very low volumetric strain with respect to Ti. Volumetric strain (here the change in volume due to expansion or collapse), should be near-zero in isovolumetrically weathered material such as saprolite.

The average of five analyses from a single corestone adjacent to the rindlets sampled was used as the protolith composition for C_w calculations of rindlet samples (Buss et al., 2008). The deepest sample (7.24 m) obtained from the augered cores on the Guaba Ridge was

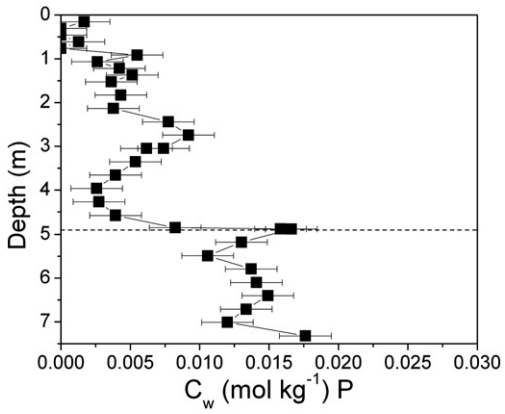

Fig. 1. Solid-state, Ti-normalized concentrations of P, C_w, with depth in the weathering profile that was sampled by augering on a ridgetop. The dashed line denotes the bottom of the saprolite. Samples below the saprolite were inferred to be rindlet zone samples on the basis of texture, color, and chemistry. Error is the standard deviation of the measured concentrations of P for five individual samples of a single corestone. The higher concentrations at ~2.5 m correspond to a visible, chemical, textural, and biological heterogeneity identified by Buss et al. (2005) as a "ghost rindlet."

used as the protolith for calculations performed on the core samples. Ti concentrations in the bedrock vary slightly throughout the watershed (Turner et al., 2003) and thus it is appropriate to use the least weathered sample obtainable under a given weathering profile as the parent material. Normalized P concentrations (C_w) increase with increasing depth into the regolith, with a dramatic increase at the bottom of the saprolite at 5 m (Fig. 1). An increase in P at approximately 2.5 m depth corresponds to a visible, biological, and chemical heterogeneity in the saprolite interpreted to be a rindlet that has not fully saprolitized: a 'ghost rindlet' (Buss et al., 2005). Below 5 m depth (where the auger penetrated the rindlet zone), normalized P concentrations range from 0.01 to 0.02 mol kg^{-1}, which is consistent with P concentrations in the rindlet zone sampled in the roadcut (Fig. 2). The gradients in C_w over the augered rindlet zone and the roadcut rindlet zone are equivalent when the rindlet zone thicknesses are scaled so that the two interfaces that delineate the rindlet zone (the saprolite–rindlet and rindlet–bedrock interfaces) coincide for both sample sets (Fig. 2).

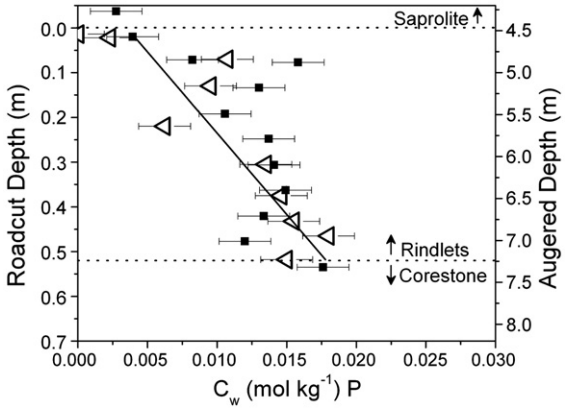

Fig. 2. Solid-state, Ti-normalized concentrations of P, C_w, in the rindlet and corestone samples collected from a roadcut (open triangles). The left-hand *y*-axis shows the distance below the saprolite–rindlet interface. A linear fit through the roadcut data is shown, which was used as the gradient in P, b_s, for calculation of the apatite weathering rate and P flux (Eqs. (3) and (5)). The equation for the regression line is $Y = 36.3X - 0.13$, $R^2 = 0.76$. Error bars are the standard deviation of the measured concentrations of P for five individual samples of a single corestone. Solid square symbols are C_w for P in the rindlet zone portion of the augered core (Fig. 1) corresponding to the right-hand *y*-axis, which shows the depth in the augered core.

Table 1
Apatite content of rindlets and corestone.

Distance[a] (cm)	Apatite[b] (vol.%)
49.0	nd[c]
48.5	nd
48.0	nd
47.5	0.01
33.0	0.14
30.0	nd
28.0	nd
21.0	0.20
16.0	0.35
8.5	0.38
5.0	0.11
4.0	0.36
0	0.62

[a] Distance from corestone.
[b] Determined by point counting backscattered electron images of thin sections using image analysis software.
[c] nd = not detected.

Dissolution of apatite within the rindlet zone is apparent in thin section as well as in the P elemental concentration profiles of the bulk materials. Loss of apatite occurs with increasing distance from the corestone–rindlet interface (Table 1). Apatite grains in the bedrock exist along grain boundaries of other minerals or as inclusions, mostly within hornblende, but also occasionally within plagioclase or primary Fe oxides. Apatite inclusions are seen to dissolve out of relatively intact crystals such as hornblende or plagioclase (Fig. 3). Phosphorus-containing secondary minerals were not detected.

Fe isotopic compositions in the HCl extracts, δ^{56}Fe, of the soil and saprolite range from about 0 to -0.1 ± 0.1‰ throughout most of the profile, consistent with values for igneous rocks (Beard et al., 2003). Only at the surface (above ~1.2 m depth) and in the deepest saprolite (at 4.9 m depth) did we observe distinct variation in isotopic compositions: values were observed to be as light as -0.64 and -0.40‰ in those zones respectively (Table 2, Fig. 4). These zones of lighter Fe isotope ratios correspond to zones of higher concentrations of extractable Fe, cell numbers, DNA yields, and Fe(II)-oxidizing bacteria (Buss et al., 2005; Fig. 4).

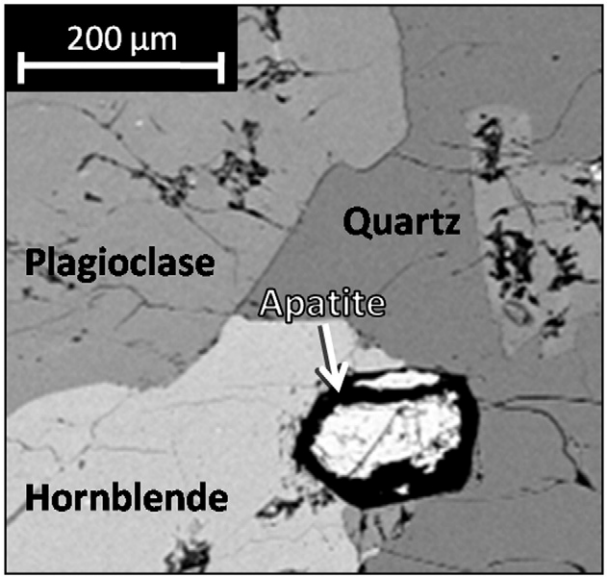

Fig. 3. Backscattered electron (BSE) image of a thin section of a rindlet from about 4 cm above the corestone sampled in a roadcut. The remnants of a dissolving apatite crystal are visible within an apatite-shaped hole. While apatite weathers across the entire 49 cm rindlet zone, hornblende only weathers within 7 cm at the saprolite–rindlet interface (Buss et al., 2008). The sample in this image is below the zone of hornblende weathering and thus the hornblende crystal appears pristine.

Table 2
Fe isotope ratios of HCl extracts.

Depth (m)	δ^{56}Fe (‰)
0.15	−0.64
0.3	−0.66
0.6	−0.55
0.9	−0.13
1.2	−0.26
2.1	−0.12
2.4	−0.08
2.4	−0.11
3.0	0.00
3.7	−0.11
4.3	−0.10
4.6	0.01
4.9	−0.40

4. Discussion

4.1. Phosphorus flux and apatite weathering

Changes in P concentration with depth in regolith generally represent depletion profiles, biogenic profiles, or depletion–addition profiles, (or a combination) (Brantley et al., 2007, 2008). A depletion profile occurs when P-bearing minerals dissolve and P is leached from the system and a biogenic profile is created when P that is solubilized at depth is transported upward and stored in the upper soil by biological processes. A depletion–addition profile is characterized by mobilization from the upper soil layer and enrichment in lower layers. A fourth type of profile is also possible: an addition profile, if atmospheric deposition or addition of P-rich fertilizers introduces P into the system. The slope of a concentration profile provides information about the rates and mechanisms of the depletion, addition, or biological processes that control the transfer of mass (e.g., White, 2002; Brantley et al., 2008; Buss et al., 2008). In the Rio Icacos watershed, the thicknesses of the weathering profiles are maintained by a positive feedback between weathering and erosion, controlled by the infiltration of aqueous O_2 to the weathering interface (Fletcher et al., 2006). Although the regolith and rindlet zones of the roadcut and augered site differ in thickness, that the concentration profiles of P in these two locations are consistent (that the same amount of P is lost from interface-to-interface, Fig. 2) points to the same mechanism of P mass transfer in both profiles.

Phosphorus in soils exists in a variety of forms, many of which are considered to be occluded or only sparingly soluble and thus not

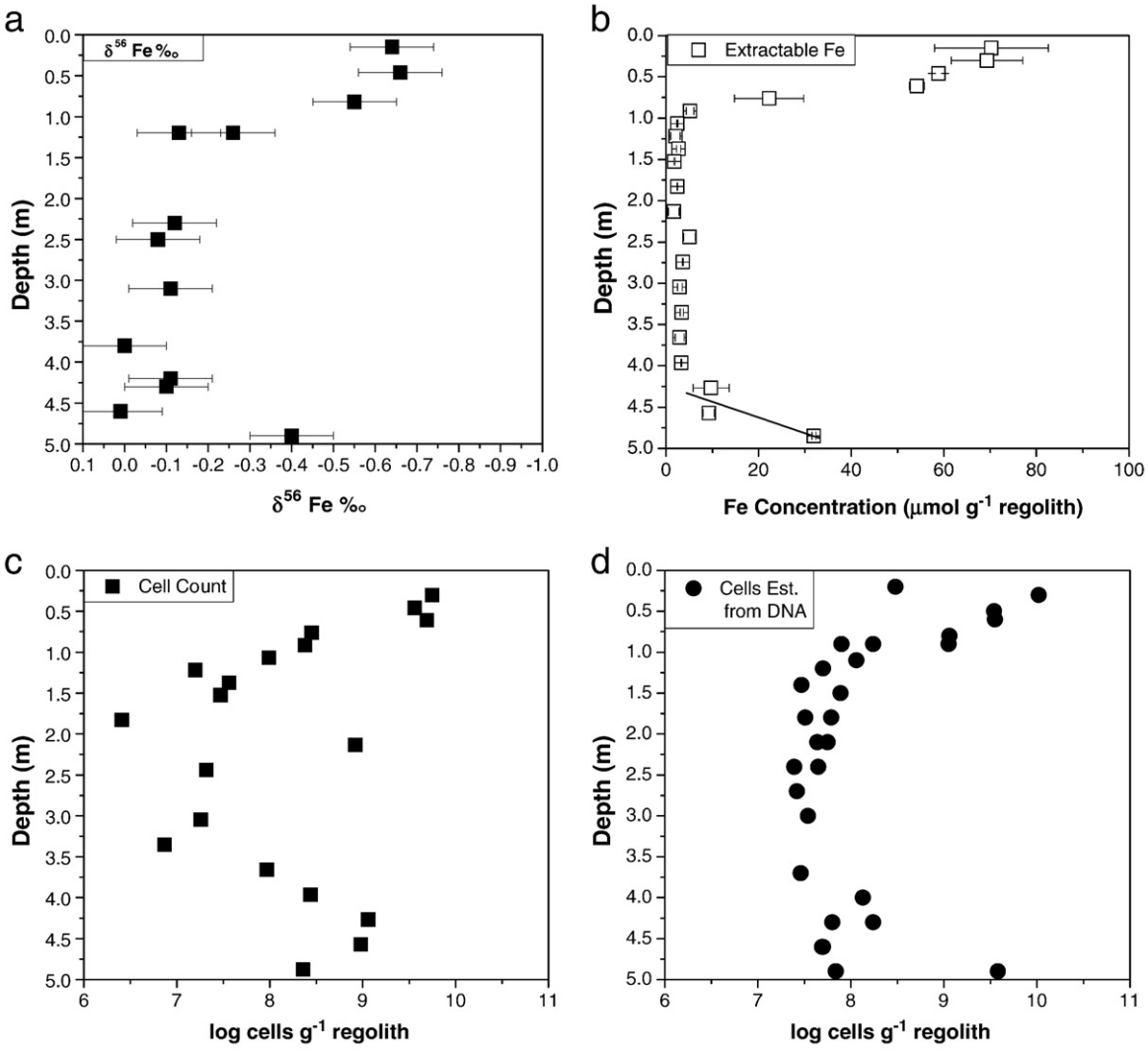

Fig. 4. a) Isotopic composition of Fe extracted with 0.5 N HCl from the soil and saprolite samples. Error is $2\sigma = 0.1$‰ calculated for multiple measurements of a goethite standard. b) Fe concentrations in 0.5 N HCl extracts (Buss et al., 2005) with a linear regression through concentrations at depths below 4 m representing the gradient in extractable Fe over this zone. Error bars are smaller than most of the symbols. c) Cell numbers estimated by direct counting (Buss et al., 2005), and d) cell numbers estimated from DNA yields (Buss et al., 2005). Notice the log scale for the cell numbers in c–d. The anomalously high cell density at ~2.2 m in c corresponds to a relatively unweathered zone in the saprolite, thought to be a "ghost rindlet" (Buss et al., 2005).

readily available to biota. However, these recalcitrant and occluded pools of P (sorbed to Al and Fe oxides, trapped within soil aggregates, or contained within clays or phosphate minerals) are slowly liberated and thus can be considered bioavailable when integrating over longer (e.g., decadal) timescales (Cumming and Weinstein, 1990; Richter et al., 2006). In addition, P sequestered in Fe(III)-(hydr)oxides can be liberated on much shorter timescales by reductive dissolution in environments subjected to redox fluctuations. In surface soils in the nearby Bisley Research Watersheds, also in the Luquillo Forest, periodic O_2 depletion (in approximately 2 week intervals) related to high biological activity, warm temperatures, and abundant rainfall, causes redox fluctuations that lead to repeated cycles of reductive dissolution and oxidative re-precipitation of Fe(III)-(hydr)oxides (Liptzin and Silver, 2009). The P released during the reductive half-cycle is immediately taken up by the biota, bypassing the "labile" P pool ($NaHCO_3$-extractable) (Liptzin and Silver, 2009). Although the deep saprolite is not subjected to the environmental fluctuations of the surface soils, microscale redox cycling at depth remains likely. Indeed, visible Mn-oxide gradients in the saprolite that are coincident with zones of high cell densities indicate local zones of redox cycling associated with microbial growth (Buss et al., 2005).

In deep saprolite profiles such as on the Guaba Ridge, where atmospheric and recycled (e.g., leaf litter) P are not available, apatite dissolution during bedrock weathering provides a source of P for the deep microbial communities. These communities are directly dependent on the flux of P from the weathering of apatite crystals in the rindlet zone. Laboratory experiments have demonstrated the ability microorganisms to enhance dissolution of apatite to obtain P (e.g., Welch et al., 2002; Schaperdoth et al., 2007) indicating that apatite-bound P can be considered a bioavailable form. In the Rio Icacos watershed, apatite weathers in the rindlet zone, often within rock layers where porosity is insufficient to host microorganisms (Fig. 3), thus microbial dissolution of apatite is not considered a dominant process relative to abiotic dissolution. Much of the P that is released by apatite dissolution is lost, as evidenced by the decline in P concentrations with decreasing depth (Figs. 1 and 2). Remaining P is either taken up by microorganisms or mineralized, most likely sorbed to Fe(III)-(hydr)oxides. Phosphorus-containing secondary minerals were not detected in the rindlet zone.

When the concentration of a mobile element (e.g., P) in a soil reflects dissolution without concomitant secondary mineral precipitation, it demonstrates a decrease in the solid-state concentration C_0 at depth z_1 to C_w at a shallower depth z_0 (White, 2002) and can be characterized as a depletion profile (Brantley et al., 2008). The slope of such a concentration–depth plot can be related to the weathering velocity, ω, or rate of advance of weathering into unaltered (parent) material, and the weathering rate, R, of the mineral supplying the mobile element. Here C_0 corresponds to the solid-state concentration of the element within the parent rock and C_w is the solid-state concentration of the element in the weathered material at depth z. While such depletion profiles often show curvature (Brantley et al., 2008), they can often be fitted satisfactorily using linear regression to calculate a slope. The reaction rate R (mol m^{-2} s^{-1}) for a given mineral in a weathering profile is calculated from the elemental distribution in the profile using the following expression from White (2002):

$$R = 10^{-3}\frac{1}{\varphi \nu s}\frac{\omega}{b_s} \tag{3}$$

where φ is the mass fraction of the mineral in the weathering material (g g^{-1}), ν is the stoichiometric coefficient of the element in the mineral (mol mol^{-1}), s is the specific surface area of the mineral (m^2 g^{-1}), b_s is the weathering gradient (m kg mol^{-1}), and ω is the weathering velocity (m s^{-1}), which is also known as the weathering advance rate or the regolith propagation rate. The weathering velocity is calculated as the thickness of the profile, Δz, divided by the time required to form the profile, t:

$$\omega = \frac{\Delta z}{t} \tag{4}$$

The methodology of White (2002) permits the calculation of solid-state reaction rates R for minerals in a weathering profile from the elemental distribution in the profile. Here we use Eq. (3) (White, 2002) to quantify a weathering rate for apatite across the rindlet zone in the Rio Icacos watershed as a function of the average weathering velocity, $\omega = 43$ m Ma^{-1} (Brown et al., 1995). We consider the gradient in P across the rindlet zone ($b_s = 36.3$ m kg mol^{-1}, Fig. 2) and mineralogical parameters $\varphi = 0.008$ g g^{-1} for apatite (determined by digital point counting and converted to mass units), and $\nu = 3$ mol P mol^{-1}. We calculate a geometric surface area, $s = 0.023$ m^2 g^{-1}, by using an average grain size of 80 μm and a cubic volume (Brantley et al., 1999). The resulting rate of apatite weathering is 6.8×10^{-14} mol m^{-2} s^{-1}, or log $R = -13.2$. This rate is several orders of magnitude slower than apatite dissolution rates measured in the laboratory (Fig. 5, Valsami-Jones et al., 1998; Welch et al., 2002; Guidry and Mackenzie, 2003), which is expected when comparing field rates to laboratory rates (White and Brantley, 2003). The only other field-based rate of apatite weathering that we are aware of is normalized to the volume of soil rather than the specific surface area of the mineral and thus cannot be directly compared (Nezat et al., 2004).

The apatite weathering profile and weathering velocity are directly related to the rate at which P is released from apatite. The flux of an element j, in terms of unit volume: F_j (mol j m^{-3} s^{-1}), can describe the rate at which apatite-derived P is supplied to the deep saprolite microbial community:

$$F_j = 10^{-3}\frac{\omega\rho}{\varphi b_s} \tag{5}$$

where j is phosphorus and ρ is the density of the weathering material, which ranges from 1.83×10^6 to 2.7×10^6 g m^{-3} over the rindlet zone (Buss et al., 2008). Using this range of density values yields: $F_P = 8.6\times10^{-9}$ to 1.3×10^{-8} mol P m^{-3} s^{-1}.

Buss et al. (2005) estimated maximum rates of microbial growth in the deepest saprolite at this site based on the flux of Fe(II) from the weathering bedrock, assuming Fe(II)-oxidizing bacteria as the dominant primary producers. These organisms are chemolithoautotrophs, that is, they use inorganic substrates for energy (e.g., Fe) and fix CO_2 to create

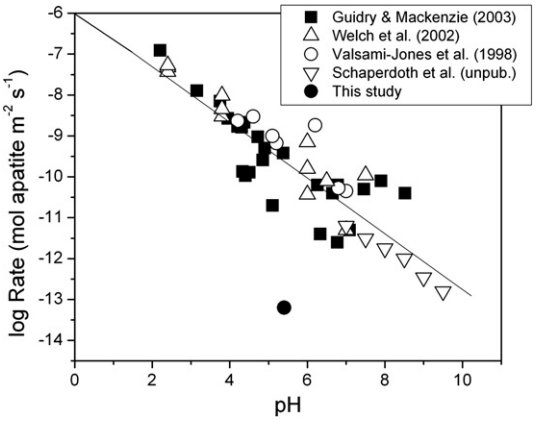

Fig. 5. Rates of apatite dissolution determined from laboratory experiments (Valsami-Jones et al., 1998; Welch et al., 2002; Guidry and Mackenzie, 2003) show a linear dependence on pH (Bandstra et al., 2008). The field rate determined in the present study is several orders of magnitude slower than the laboratory rates. Laboratory rates are normalized to BET surface area of the mineral. The field rate is normalized to a geometric mineral surface area. The field pH of 5.4 was measured by White et al. (1998) in porewater on the Guaba Ridge.

organic carbon (autotrophy). The calculated growth rates, β, were 6.9×10^{-8} mol biomass C m^{-3} s^{-1} for Fe(II)-oxidizing bacteria and 3.5×10^{-8} mol C m^{-3} s^{-1} for heterotrophic bacteria. These latter bacteria are dependent on the organic carbon produced by the Fe(II)-oxidizers because the dissolved organic carbon (DOC) in porewaters at these depths is extremely low: 125 μM (Murphy, 1995) and therefore the flux of DOC from the surface is insignificant relative to the flux of organic carbon produced by autotrophy: ~10^{-7} vs 10^{-4} mol C m^{-3} h^{-1}, respectively (Buss et al., 2005).

To estimate the flux of P required, F_{req} (mol P m^{-3} s^{-1}), to maintain a given growth rate, β (mol C m^{-3} s^{-1}), we divide the growth rate by the molar C:P ratio of the cells, X (mol mol^{-1}):

$$F_{req} = \frac{\beta}{X} \tag{6}$$

The molar C:P ratio measured mixed cultures of P-limited lakewater heterotrophic bacteria has been reported to lie in the range 80:1 to100:1 (Jurgens and Gude, 1990). Other values in the literature range from 57:1 to 100:1 for several individual species of P-limited, non-marine, environmental bacteria (Jurgens and Gude, 1990). Taking a C:P ratio of 100 as a rough estimate, we can use Eq. (6) to estimate the flux of P required to support microbial growth at the rates calculated by Buss et al. (2005): $F_{req} = 6.9\times10^{-10}$ and 3.5×10^{-10} mol P m^{-3} s^{-1} for the Fe(II)-oxidizing and heterotrophic communities, respectively. These fluxes are less than the flux of P provided by apatite weathering, F_P (Eq. (5)). Phosphorus requirements vary among specific organisms and therefore we may be underestimating F_{req}, but because actual growth rates are expected to be lower than the maximum rates estimated by Buss et al. (2005), these results suggest that P is not limiting at the saprolite–bedrock interface.

4.2. Fe isotopic composition of the regolith profile

The HCl extraction is expected to liberate aqueous Fe; Fe contained within microorganisms and biofilms; and weakly sorbed, amorphous, or poorly crystalline solid Fe (Emerson, 2002; Buss et al., 2005; Wiederhold et al., 2007b). Thus we consider two general reservoirs of Fe in the weathering profile: the extractable reservoir and the non-extractable reservoir, which contains well-crystallized phases including Fe-silicates and goethite. Significant sequestration of Fe in recalcitrant organic material is unlikely because concentrations of organic C are extremely low below 1 m depth (Buss et al., 2005).

An enrichment of light Fe isotopes, such as we measured at the top and bottom of the Rio Icacos weathering profile, is created by preferential input of ^{54}Fe to the extractable reservoir, preferential removal of ^{56}Fe, or both. At the bottom of the saprolite, input to the reservoir of HCl-extractable Fe is dominated by complete and rapid dissolution of hornblende, which occurs only within a 7 cm zone at the rindlet–saprolite interface (Buss et al., 2008). Inorganic dissolution of hornblende does not produce a fractionation in Fe isotopes in laboratory experiments; however, dissolution of hornblende in the presence of organic acids, siderophores, or bacteria preferentially releases ^{54}Fe via a kinetic isotope effect, producing a solution that is as much as 0.8‰ lighter than the mineral (Brantley et al., 2001a, 2004). Organic dissolution of hornblende is thus consistent with the enrichment in light Fe isotopes and the higher cell densities at the bedrock–saprolite interface. Although the Rio Icacos weathering profile is characterized by oxidation processes (White et al., 1998; Buss et al., 2005; Fletcher et al., 2006; Buss et al., 2008) and neither Fe (III)-reducing bacteria nor redoximorphic features (e.g., mottling) have been detected in the saprolite (Buss et al., 2005), reductive dissolution cannot be entirely ruled out. Microaerophilic, circumneutral Fe(II)-oxidizing bacteria were found in the deep saprolite (Buss et al., 2005), which implies that oxygen may be depleted at depth, possibly within microenvironments. Microscale redox cycling of Fe by bacteria has been demonstrated in circumneutral sediments (Sobolev and Roden, 2002; Roden et al., 2004). Regardless, the rapid dissolution of hornblende clearly dominates Fe input to the extractable reservoir at the bedrock–saprolite interface.

Isotopically light extractable Fe also correlates with a larger reservoir of HCl-extractable Fe and high cell densities in the top meter of the weathering profile, which comprises the soil and rooting zone. Organic dissolution of biotite (and possibly Fe-bearing dust), decomposition of isotopically light vegetation, and microbial or plant-mediated reductive dissolution of Fe(III)-(hydr)oxides may all contribute to inputs of isotopically light Fe to the HCl-extractable reservoir in the surface soil.

The higher concentration of Fe in the HCl extracts at the top and bottom of the profile relative to the middle saprolite indicates that input to the reservoir of extractable Fe is faster than output from the reservoir in these zones. Organic dissolution of hornblende by organic ligands or bacteria is substantially faster than inorganic dissolution (Kalinowski et al., 2000; Liermann et al., 2000; Brantley et al., 2001b, 2004; Buss et al., 2007), producing a “pulse” of isotopically light Fe at the start of the hornblende weathering process. Calculations of C_w for Fe in the saprolite and rindlets (Buss et al., 2005, 2008) are approximately constant with depth, indicating that Fe is conserved within the system. Therefore, the only mechanism for removing Fe from the extractable reservoir is by sequestration within well-crystallized Fe(III)-(hydr)oxides either by re-crystallization of ferrihydrite to form goethite or hematite or possibly diffusion of sorbed Fe into the crystalline phases. The rate of crystallization is a function of the concentration of the ferrihydrite precursor, but can be affected by redox cycling and sorption processes. Repeated redox cycling of Fe has been shown to increase the crystallinity of Fe(III)-(hydr)oxides and decrease the size of the HCl-extractable Fe reservoir (Thompson et al., 2006). However, the formation of goethite can be retarded by the sorption onto ferrihydrite of organic acids including citrate and meso-tartrate, simple sugars including glucose and maltose, and silicate ions (Cornell, 1987). In contrast, adsorption of Fe(II) onto ferrihydrite substantially accelerates the formation of goethite, likely because it can act as a reductant, encouraging dissolution of ferrihydrite (Yee et al., 2006). A sorbed Fe(II) atom oxidizes and precipitates as goethite, while a ferrihydrite Fe(III) atom is reduced and propagates the process. Because the heavier isotope preferentially partitions into the oxidized product during equilibrium isotope exchange between Fe(II) and Fe(III), this process could contribute to the isotopically light signature of the extractable reservoir (Icopini et al., 2004), allowing it to persist for some time after the dissolving hornblende becomes depleted in ^{54}Fe. Although batch experiments demonstrated rapid isotopic equilibration between poorly crystalline and well-crystallized Fe(III)-hydroxides when exposed to Fe(II) (Pedersen et al., 2005), such equilibration is expected to be significantly slower in the hydrologically unsaturated (vadose zone) saprolite. Unlike surface soils, the deep saprolite is not chemically or hydrologically affected by precipitation events or seasonal cycles and thus the chemical composition, moisture content, O_2 partial pressure, and reaction rates are stable over relatively long timescales in the deep saprolite (White et al., 1998), at least at the bulk sampling scale (i.e., there may be more variability within microenvironments). However, the potential for Fe isotopic transience in the HCl-extractable reservoir due to aqueous Fe(II)-exchange with Fe(III)-hydroxides or repeated redox cycling of Fe (Thompson et al., 2006) should be noted.

Biological activity at the bedrock–saprolite interface and in the surface soil may slow the output of Fe from the extractable reservoir by organic complexation of Fe in solution or sorption of microbial products such as organic acids or sugars onto ferrihydrite. However, once the input of Fe from hornblende dissolution (which becomes isotopically heavier as dissolution progresses) is exhausted, it is only a matter of time before the extractable Fe crystallizes into a non-extractable form, homogenizing the two isotopic pools into a single reservoir. Without the

large flux of Fe from the dissolution of hornblende (Buss et al., 2008), active microbial communities can no longer be supported and this is reflected in the low cell densities, extremely low extractable Fe concentration, and near-zero δ^{56}Fe within the middle saprolite. In the saprolite, Fe exists within oxide minerals and biotite, which weathers to kaolinite throughout the saprolite (Murphy et al., 1998). The very low concentrations of HCl-extractable Fe in the middle saprolite may also reflect a history of redox cycles at the rindlet–saprolite interface, which can decrease the size of this pool (Thompson et al., 2006). It is also relevant to note that redox cycling of Fe increases the bioavailability of P (Liptzin and Silver, 2009), which is often sorbed to Fe(III)-(hydr)oxides in soil and saprolite.

We can estimate the flux of Fe into the extractable reservoir due to hornblende weathering using Eq. (5). The gradient, b_s, in total Fe(II) across the zone of hornblende weathering, which occurs over 7 cm at the bedrock–rindlet interface, is $b_s = 0.088$ m kg mol^{-1} (Buss et al., 2008), $\varphi = 0.063$ g g^{-1} (White et al., 1998), and $\rho = 1.83 \times 10^6$ g m^{-3} in the deep saprolite (White et al., 1998). The resulting flux, $F_{Fe} = 4.5 \times 10^{-7}$ mol Fe m^{-3} s^{-1}. This rate of input can be compared to the rate of output via goethite crystallization using Eq. (5) and the gradient in extractable Fe in the deep saprolite, $b_s = 19.01$ m kg mol^{-1} (Fig. 4b), and $\varphi = 0.0018$ g g^{-1} (Buss et al., 2005). The resulting Fe flux out, $-F_{Fe} = 7.3 \times 10^{-8}$ mol Fe m^{-3} s^{-1}, is an order of magnitude slower than the Fe flux in due to hornblende dissolution. This result is consistent with the observation that the extractable reservoir reaches the isotopic value of the middle saprolite before (at ~4.6 m depth) it reaches the concentration value of the middle saprolite (at ~4.0 m depth).

Enhanced dissolution of hornblende by organic ligands, suggested by the isotopic and concentration gradients in extractable Fe at the bedrock–saprolite interface, indicates an active role for biota in chemical weathering. In addition to increasing the rate of hornblende dissolution, organic ligands produced by microorganisms may increase the rate of other mineral weathering reactions by lowering the pH of the porefluids. Furthermore, microbial consumption of oxygen during respiration may affect the rate of spheroidal fracturing, which is thought to be controlled by the concentration of oxygen in the porewater (Fletcher et al., 2006). These results raise the possibility of a "bio-limited" weathering profile in which a change in the rate of biogeochemical weathering would lead to a change in the total denudation rate. Weathering systems are typically classified as either weathering-limited or transport-limited (Stallard, 1992; Kump et al., 2000; Riebe et al., 2004; West et al., 2005). In a weathering-limited regime, total denudation is controlled by the chemical weathering rate, which is limited by the kinetics of mineral weathering reactions. In contrast, in a transport-limited regime (also called supply-limited), the total denudation rate is controlled by the rate of erosion. In the transport-limited case, perturbations in the weathering rate do not affect the total denudation rate because the weathering rate is high relative to the erosion rate; development of a thick regolith is a consequence. Because the Rio Icacos weathering profile is consistent with models of transport-limitation (Fletcher et al., 2006; Lebedeva et al., 2007), it is unlikely that microbial influence on the weathering rate would affect the denudation rate or the thickness of the regolith profile studied here. However, it is interesting to note that a weathering-limited profile could also be bio-limited.

5. Conclusions

Iron in HCl extracts of saprolite samples is slightly fractionated relative to igneous rocks through the majority of a saprolite profile overlying quartz diorite in the Luquillo Mountains, Puerto Rico: δ^{56}Fe values generally range from approximately 0 to −0.1‰. However, HCl-extractable Fe is significantly enriched in the lighter isotope in samples taken from the soil and from the bottom of the saprolite directly overlying the bedrock, where δ^{56}Fe = −0.64 and −0.40‰, respectively. These zones of lighter Fe isotopic compositions are consistent with the zones of highest biological activity in the saprolite as measured by cell density. Whereas organisms in the soil are generally heterotrophic and can thrive on relatively abundant organic carbon in the soil and porewaters, little to no organic carbon is available at the bedrock–saprolite interface, other than cellular material. Microorganisms at the bottom of the saprolite therefore rely on Fe and P released from the spheroidally weathering bedrock as an energy and nutrient source, respectively, with Fe as the limiting "nutrient." The bedrock–saprolite interface is characterized by spheroidal fractures that delineate ~2.5-cm thick rindlets and that comprise ~50-cm thick rindlet sets. Apatite is present in the corestone at parent abundance, but is not measured in the saprolite: we calculate that apatite weathers across the rindlet sets at a rate of 6.8×10^{-14} mol m^{-2} s^{-1}. Using growth yields from the literature and weathering release rates of Fe(II), biomass production rates were calculated previously by Buss et al. (2005). The apatite dissolution rate calculated here produces a flux of P sufficient to support these growth rates. Therefore our results suggest that P is not limiting at the saprolite–bedrock interface. These results are consistent with the conclusion, advanced in our earlier paper, that the ecosystem that survives at ~5 m depth in the saprolite directly above the bedrock in the Rio Icacos weathering profile is dependent upon chemolithoautotrophic primary producers. These chemolithoautotrophs are Fe(II) oxidizers and are sustained through Fe released from the weathering bedrock. Active cycling of Fe by microorganisms is reflected in the isotopically light Fe in the HCl extracts from the top and bottom of the weathering profile, although the cycling and fractionation mechanisms may differ between the surface and deep ecosystems. The preferential mobilization of light Fe isotopes at the bedrock–saprolite interface suggests that microorganisms are likely influencing concentrations of Fe and oxygen in the porewater and thus affecting the rates of weathering of Fe-bearing minerals.

Acknowledgements

We thank Lisa Stillings, Aaron Thompson, Tom Bullen, and two anonymous reviewers for thoughtful comments that improved the manuscript, R.C. Fletcher, J. Troester, and M. Rosario-Torres for field assistance and J. Kittleson, G. Icopini, M. Angelone, G. Hart, and J. Vervoort for laboratory and data assistance. Funding provided by DOE grant no. DE-FG02-05ER15675, the Penn State Biogeochemical Research Initiative for Education (BRIE) supported by NSF-IGERT grant no. DGE-9972759, and the Water Energy and Biogeochemical Budgets Program of the U.S. Geological Survey. H.L. Buss acknowledges fellowship support of the NSF Graduate Research Fellowship Program and the National Academy of Sciences Research Associateship Program.

References

Anderson, S.P., Dietrich, W.E., Brimhall, G.H., 2002. Weathering profiles, mass-balance analysis, and rates of solute loss: linkages between weathering and erosion in a small, steep catchment. Geol. Soc. Am. Bull. 114, 1143–1158.

Arnold, G.L., Anbar, A.D., Barling, J., Lyons, T.W., 2004. Molybdenum isotope evidence for widespread anoxia in mid-Proterozoic oceans. Science 304 (5667), 87–90.

Bandstra, J.Z., Buss, H.L., Campen, R.K., Liermann, L.J., Moore, J., Hausrath, E.M., Navarre-Sitchler, A.K., Jang, J.-H., Brantley, S.L., 2008. Appendix: compilation of mineral dissolution rates. In: Brantley, S.L., Kubicki, J.D., White, A.F. (Eds.), Kinetics of Water–Rock Interaction. Springer, New York, pp. 737–823.

Beard, B.L., Johnson, C.M., Cox, L., Sun, H., Nealson, K.H., Aguilar, C., 1999. Iron isotope biosignatures. Science 285, 1889–1892.

Beard, B.L., Johnson, C.M., Skulan, J.L., Nealson, K.H., Cox, L., Sun, H., 2003. Application of Fe isotopes to tracing the geochemical and biological cycling of Fe. Chem. Geol. 195, 87–117.

Boccheciamp, R.A., Rivera, W.F., Trigo, J.E., Brunet, J.E., Torres, E.O., McKinze, W.E., Rivera, L.H., 1977. Soil Survey of the Humacao Area of Eastern Puerto Rico. USDA Soil Conservation Service, Washington, D.C.

Brantley, S.L., White, A.F., Hodson, M., 1999. Specific surface area of primary silicates. In: Jamtveit, B., Meakin, P. (Eds.), Growth and Dissolution in Geosystems. Kluwer Academic Publishers, Dordrecht, pp. 291–326.

Brantley, S.L., Bullen, T.D., Liermann, L., 2001a. Fractionation of Fe isotopes by soil microbes and organic acids. Geology 29, 535–538.
Brantley, S.L., Liermann, L., Bullen, T.D., 2001b. Fractionation of Fe isotopes by soil microbes and organic acids. Geology 29 (6), 535–538.
Brantley, S.L., Liermann, L.J., Guynn, R.L., Anbar, A., Icopini, G.A., Barling, J., 2004. Iron isotope fractionation during mineral dissolution with and without bacteria. Geochim. Cosmochim. Acta 68 (15), 3189–3204.
Brantley, S.L., Goldhaber, M.B., Ragnarsdottir, K.V., 2007. Crossing disciplines and scales to understand the critical zone. Elements 3, 307–314.
Brantley, S.L., Bandstra, J., Moore, J., White, A.F., 2008. Modelling chemical depletion profiles in regolith. Geoderma 145, 494–504.
Brimhall, G., Dietrich, W.E., 1987. Constitutive mass balance relations between chemical composition, volume, density, porosity, and strain in metasomatic hydrochemical systems: results on weathering and pedogenisis. Geochim. Cosmochim. Acta 51, 567–587.
Brown, E.T., Stallard, R., Larsen, M.C., Raisbeck, G.M., Yiou, F., 1995. Denudation rates determined from the accumulation of in situ-produced 10Be in the Luquillo Experimental Forest, Puerto Rico. Earth Planet. Sci. Lett. 129, 193–202.
Bruijnzeel, L.A., 1991. Nutrient input–output budgets of tropical forest ecosystems: a review. J. Trop. Ecol. 7 (1), 1–24.
Bullen, T.D., White, A.F., Childs, C.W., Vivit, D.V., Schulz, M.S., 2001. Demonstration of significant abiotic iron isotope fractionation in nature. Geology 29 (8), 699–702.
Buss, H.L., Sak, P.B., White, A.F., Brantley, S.L., 2004. Mineral dissolution at the granite–saprolite interface. In: Wanty, R.B., Seal, R.R.I. (Eds.), 11th International Symposium on Water–Rock Interaction. Taylor and Francis, Saratoga Springs, NY, pp. 819–823.
Buss, H.L., Bruns, M.A., Schultz, M.J., Moore, J., Mathur, C.F., Brantley, S.L., 2005. The coupling of biological iron cycling and mineral weathering during saprolite formation, Luquillo Mountains, Puerto Rico. Geobiology 3 (4), 247–260.
Buss, H.L., Luttge, A., Brantley, S.L., 2007. Etch pit formation on iron silicate surfaces during siderophore-promoted dissolution. Chem. Geol. 240, 326–342.
Buss, H.L., Sak, P.B., Webb, S.M., Brantley, S.L., 2008. Weathering of the Rio Blanco quartz diorite, Luquillo Mountains, Puerto Rico: coupling oxidation, dissolution, and fracturing. Geochim. Cosmochim. Acta 72, 4488–4507.
Chadwick, O.A., Brimhall, G.H., Hendricks, D.M., 1990. From black box to a grey box: a mass balance interpretation of pedogenesis. Geomorphology 3, 369–390.
Cornell, R.M., 1987. Comparison and classification of the effects of simple ions and molecules upon the transformation of ferrihydrite into more crystalline products. Z. Pflanzenernahr. Bodenk. 150, 304–307.
Crosby, H.A., Johnson, C.M., Roden, E.E., Beard, B.L., 2005. Coupled Fe(II)–Fe(III) electron and atom exchange as a mechanism for Fe isotope fractionation during dissimilatory iron oxide reduction. Environ. Sci. Technol. 39, 6698–6704.
Crosby, H.A., Roden, E.E., Johnson, C.M., Beard, B.L., 2007. The mechanisms of iron isotope fractionation produced during dissimilatory Fe(III) reduction by Shewanella putrefaciens and geobacter sulfurreducens. Geobiology 5, 169–189.
Cumming, J.R., Weinstein, L.H., 1990. Utilization of AlPO4 as a phosphorus source by ectomycorrhizal Pinus rigida mill. seedlings. New Phytol. 116, 99–106.
Dixon, J.C., Campbell, S.W., Thorn, C.E., Darmody, R.G., 2006. Incipient weathering rind development on introduced machine-polished granite discs in an Arctic alpine environment, northern Scandinavia. Earth Surf. Proc. Landforms 31, 111–121.
Dorn, R., 1995. Digital processing of back-scatter electron imagery: a microscopic approach to quantifying chemical weathering. Geol. Soc. Am. Bull. 107, 725–741.
Emerson, D., 2002. Microbial oxidation of Fe(II) and Mn(II) at circumneutral pH. In: Lovely, D.R. (Ed.), Environmental Microbe–Metal Interactions. ASM, Washington D.C.
Fantle, M.S., DePaolo, D.J., 2004. Iron isotopic fractionation during continental weathering. Earth Planet. Sci. Lett. 228, 547–562.
Fletcher, R.C., Buss, H.L., Brantley, S.L., 2006. A spheroidal weathering model coupling porewater chemistry to soil thicknesses during steady-state denudation. Earth Planet. Sci. Lett. 244, 444–457.
Frausto da Silva, J.J.R., Williams, R.J.P., 1991. The Biological Chemistry of the Elements. Clarendon Press, Oxford, UK. 561 pp.
Frizano, J., Johnson, A.H., Vann, D.R., 2002. Soil phosphorus fractionation during forest development on landslide scars in the Luquillo Mountains, Puerto Rico. Biotropica 34 (1), 17–26.
Garrett, R.H., Grisham, C.M., 1999. Biochemistry. Harcourt Brace College Publishers, Orlando. 1127 pp.
Graham, R.C., Duce, R.A., 1982. The atmospheric transport of phosphorus to the western North Atlantic. Atmos. Environ. 16 (5), 1089–1097.
Guelke, M., Von Blanckenburg, F., 2007. Fractionation of stable iron isotopes in higher plants. Environ. Sci. Technol. 41, 1896–1901.
Guidry, M.W., Mackenzie, F.T., 2003. Experimental study of igneous and sedimentary apatite dissolution: control of pH, distance from equilibrium, and temperature on dissolution rates. Geochim. Cosmochim. Acta 67 (16), 2949–2963.
Heartsill-Scalley, T., Scatena, F.N., Estrada, C., McDowell, W.H., Lugo, A.E., 2007. Disturbance and long-term patterns of rainfall and throughfall nutrient fluxes in a subtropical wet forest in Puerto Rico. J. Hydrol. 333, 472–485.
Icopini, G.A., Anbar, A.D., Ruebush, S.S., Tien, M., Brantley, S.L., 2004. Iron isotope fractionation during microbial reduction of iron; the importance of adsorption. Geology 32 (3), 205–208.
Jurgens, K., Gude, H., 1990. Incorporation and release of phosphorus by planktonic bacteria and phagotrophic flagellates. Mar. Ecol. Prog. Ser. 59, 271–284.
Kalinowski, B.E., Liermann, L.J., Brantley, S.L., Barnes, A., Pantano, C.G., 2000. X-ray photoelectron evidence for bacteria-enhanced dissolution of hornblende. Geochim. Cosmochim. Acta 64 (8), 1331–1343.
Kump, L.R., Brantley, S.L., Arthur, M.A., 2000. Chemical weathering, atmospheric CO2 and climate. Ann. Rev. Earth Planet. Sci. 28, 611–667.
Kurtz, A.C., Derry, L.A., 2004. Tracing silicate weathering and terrestrial silica cycling with Ge/Si ratios. In: Wanty, R.B., Seal, R.R.I. (Eds.), The 11th International Symposium on Water–Rock Interaction. A.A. Balkema, Saratoga Springs, NY, pp. 833–840.
Lebedeva, M.I., Fletcher, R.C., Balashov, V.N., Brantley, S.L., 2007. A reactive diffusion model describing transformation of bedrock to saprolite. Chem. Geol. 244, 624–645.
Liermann, L.J., Kalinowski, B.E., Brantley, S.L., Ferry, J.G., 2000. Role of bacterial siderophores in dissolution of hornblende. Geochim. Cosmochim. Acta 64 (4), 587–602.
Liptzin, D., Silver, W.L., 2009. Effects of carbon additions on iron reduction and phosphorus availability in a humid tropical forest soil. Soil Biol. Biochem. 41 (8), 1696–1702. doi:10.1016/j.soilbio.2009.05.013.
Lugolobi, F., Kurtz, A.C., Salvucci, G.D., 2006. Silica Sources and Water Flowpaths During Storm Events at Rio Icacos, Puerto Rico. Eos Trans. AGU, 87 (52): Fall Meet. Suppl., Abstract H11I-01.
Maréchal, C.N., Télouk, P., Albarède, F., 1999. Precise analysis of copper and zinc isotopic compositions by plasma-source mass spectrometry. Chem. Geol. 156, 251–273.
McDowell, W.H., Asbury, C.E., 1994. Export of carbon, nitrogen, and major ions from three tropical montane watersheds. Limnol. Oceanogr. 39 (1), 111–125.
Muhs, D.R., Budahn, J.R., Prospero, J.M., Carey, S.N., 2007. Geochemical evidence for African dust inputs to soils of western Atlantic islands: Barbados, the Bahamas, and Florida. J. Geophys. Res. 112, F02009.
Murphy, S.F., 1995. Weathering of Biotite in a Tropical Forest Soil, Luquillo Mountains, Puerto Rico. M.S. Thesis, The Pennsylvania State University, University Park, PA, 100 pp.
Murphy, S.F., Brantley, S.L., Blum, A.E., White, A.F., Dong, H., 1998. Chemical weathering in a tropical watershed, Luquillo Mountains, Puerto Rico; II. Rate and mechanism of biotite weathering. Geochim. Cosmochim. Acta 62 (2), 227–243.
Nezat, C.A., Blum, J.D., Klaue, A., Johnson, C.E., Siccama, T.G., 2004. Influence of landscape position and vegetation on long-term weathering rates at the Hubbard Brook Experimental Forest, New Hampshire, USA. Geochim. Cosmochim. Acta 68 (14), 3065–3078.
Olander, L.P., Vitousek, P.M., 2005. Short-term controls over inorganic phosphorus during soil and ecosystem development. Soil Biol. Biochem. 37, 651–659.
Pedersen, H.D., Postma, D., Jakobsen, R., Larsen, O., 2005. Fast transformation of iron oxyhydroxides by the catalytic action of aqueous Fe(II). Geochim. Cosmochim. Acta 69, 3967–3977.
Pett-Ridge, J., 2009. Contributions of dust to phosphorus cycling in tropical forests of the Luquillo Mountains, Puerto Rico. Biogeochemistry 94 (1), 63–80.
Pett-Ridge, J.C., Derry, L.A., Kurtz, A.C., 2009. Sr isotopes as a tracer of weathering processes and dust inputs in a tropical granitoid watershed, Luquillo Mountains, Puerto Rico. Geochim. Cosmochim. Acta 73, 25–43.
Richter, D.D., Allen, H., Li, J., Markewitz, D., Raikes, J., 2006. Bioavailability of slowly cycling soil phosphorus: major restructuring of soil P fractions over four decades in an aggrading forest. Oecologia 150 (2), 259–271.
Riebe, C.S., Kirchner, J.W., Finkel, R.C., 2004. Erosional and climatic effects on long-term chemical weathering rates in granitic landscapes spanning diverse climate regimes. Earth Planet. Sci. Lett. 224, 547–562.
Roden, E.E., Sobolev, D., Glazer, B., Luther III, G.W., 2004. Potential for microscale bacterial Fe redox cycling at the aerobic–anaerobic interface. Geomicrobiology 21 (6), 379–391.
Sanchez, P.A., 1976. Properties and Management of Soils in the Tropics. Wiley, New York. 618 pp.
Schaperdoth, I., Liermann, L., Brantley, S., 2007. The effect of polymeric substances on apatite reactivity in the presence of a freshwater cyanobacterium. Geomicrobiol. J. 24 (2), 79–91.
Severmann, S., Johnson, C.M., Beard, B.L., McManus, J., 2006. The effect of early diagenesis on the Fe isotope compositions of porewaters and authigenic minerals in continental margin sediments. Geochim. Cosmochim. Acta 70, 2006–2022.
Simon, A., Larsen, M.C., Hupp, C.R., 1990. The role of soil processes in determining mechanisms of slope failure and hillslope development in a humid-tropical forest, eastern Puerto Rico. Geomorphology 3, 263–286.
Skulan, J.L., Beard, B.L., Johnson, C.M., 2002. Kinetic and equilibrium Fe isotope fractionation between aqueous Fe(III) and hematite. Geochim. Cosmochim. Acta 66 (17), 2995–3015.
Sobolev, D., Roden, E.E., 2002. Evidence for rapid microscale bacterial redox cycling of iron in circumneutral environments. Antonie van Leeuwenhoek 81 (587–597).
Stallard, R.F., 1992. Tectonic processes, continental freeboard, and the rate-controlling step for continental denudation. In: Butcher, S.S., Charlson, R.J., Orians, G.H., Wolfe, G.V. (Eds.), Global Biogeochemical Cycles. Academic Press, London, pp. 93–121.
Templer, P.H., Silver, W.L., Pett-Ridge, J., DeAngelis, K.M., Firestone, M.K., 2008. Plant and microbial controls on nitrogen retention and loss in a humid tropical forest. Ecology 89 (11), 3030–3040.
Teutsch, N., von Gunten, U., Porcelli, D., Cirpka, O.A., Halliday, A.N., 2005. Adsorption as a cause for iron isotope fractionation in reduced groundwater. Geochim. Cosmochim. Acta 17 (1), 4175–4185.
Thompson, A., Chadwick, O.A., Rancourt, D.G., Chorover, J., 2006. Iron-oxide crystallinity increases during soil redox oscillations. Geochim. Cosmochim. Acta 70, 1710–1727.
Thompson, A., Ruiz, J., Chadwick, O.A., Titus, M., Chorover, J., 2007. Rayleigh fractionation of iron isotopes during pedogenesis along a climate sequence of Hawaiian basalt. Chem. Geol. 238, 72–83.
Turner, B., 2001. Effects of Temperature and Climate on Chemical Weathering in Two Contrasting High-Rainfall Mountainous Catchments. Ph.D. Thesis, Pennsylvania State University, University Park, PA.
Turner, B.F., Stallard, R.F., Brantley, S.L., 2003. Investigation of in situ weathering of quartz diorite bedrock in the Rio Icacos basin, Luquillo Experimental Forest, Puerto Rico. Chem. Geol. 202 (3–4), 313–341.

USDA NCRS, 2002. Soil Survey of Caribbean National Forest and Luquillo Experimental Forest, Commonwealth of Puerto Rico. USDA, Natural Resources Conservation Service, Washington D.C., p. 181.
Valsami-Jones, E., Ragnarsdottir, K.V., Putnis, A., Bosbach, D., Kemp, A.J., Cressey, G., 1998. The dissolution of apatite in the presence of aqueous metal cations at pH 2–7. Chem. Geol. 151, 215–233.
Vitousek, P.M., 1984. Litterfall, nutrient cycling, and nutrient limitation in tropical forests. Ecology 65 (1), 285–298.
Vitousek, P.M., Sanford Jr., R.L., 1986. Nutrient cycling in moist tropical forest. Ann. Rev. Ecol. Syst. 17, 137–167.
Walker, T.W., Syers, J.K., 1976. Fate of phosphorus during pedogenesis. Geoderma 15 (1), 1–19.
Wardle, D.A., Walker, L.R., Bardgett, R.D., 2004. Ecosystem properties and forest decline in contrasting long-term chronosequences. Science 305 (5683), 509–513.
Welch, S.A., Taunton, A.E., Banfield, J.F., 2002. Effect of microorganisms and microbial metabolites on apatite dissolution. Geomicrobiol. J. 19 (3), 343–367.
West, A.J., Galy, A., Bickle, M., 2005. Tectonic and climatic controls on silicate weathering. Earth Planet. Sci. Lett. 235, 211–228.
White, A.F., 2002. Determining mineral weathering rates based on solid and soute weathering gradients and velocities: application to biotite weathering in saprolites. Chem. Geol. 190, 69–89.
White, A.F., Brantley, S.L., 2003. The effect of time on the experimental and natural weathering rates of silicate minerals. Chem. Geol. 202, 479–506.
White, A.F., Blum, A.E., Schulz, M.S., Vivit, D.V., Stonestrom, D.A., Larsen, M., Murphy, S.F., Eberl, D., 1998. Chemical weathering in a tropical watershed, Luquillo Mountains, Puerto Rico: I. Long-term versus short-term weathering fluxes. Geochim. Cosmochim. Acta 62 (2), 209–226.
Wiederhold, J.G., Kraemer, S.M., Teutsch, N., Borer, P.M., Halliday, A.N., Kretzschmar, R., 2006. Iron isotope fractionation during proton-promoted, ligand-controlled, and reductive dissolution of goethite. Environ. Sci. Technol. 40, 3787–3793.
Wiederhold, J.G., Teutsch, N., Kraemer, S.M., Halliday, A.N., Kretzschmar, R., 2007a. Iron isotope fractionation during pedogenesis in redoximorphic soils. Soil Sci. Soc. Am. J. 71 (6), 1840–1850.
Wiederhold, J.G., Teutsch, N., Kraemer, S.M., Halliday, A.N., Kretzschmar, R., 2007b. Iron isotope fractionation in oxic soils by mineral weathering and podzolization. Geochim. Cosmochim. Acta 71, 5821–5833.
Yee, N., Shaw, S., Benning, L.G., Nguyen, T.H., 2006. The rate of ferrihydrite transformation to goethite via the Fe(II) pathway. Am. Mineral. 91, 92–96.
Zarin, D.J., Johnson, A.H., 1995. Base saturation, nutrient cation, and organic matter increases during early pedogenesis on landslide scars in the Luquillo Experimental Forest, Puerto Rico. Geoderma 65, 317–330.
Ziegler, K., Chadwick, O.A., White, A., Brzezinski, M.A., 2005. d30Si systematics in a granitic saprolite, Puerto Rico. Geology 33 (10), 817–820.